Journal of Membrane Science 720 (2025) 123782

Contents lists available at ScienceDirect

Journal of Membrane Science

journal homepage: www.elsevier.com/locate/memsci

Selective separation of acetylene from ethylene using mixed matrix membranes with MIL-100(Fe) as a filler

Nitasha Habib [a,b], Ahmet Safa Aydogdu [a,b], Seda Keskin [a,b,**], Alper Uzun [a,b,c,*]

[a] Department of Chemical and Biological Engineering, Koç University, Rumelifeneri Yolu, Sariyer, 34450, Istanbul, Türkiye
[b] Koç University TÜPRAŞ Energy Center (KUTEM), Koç University, Rumelifeneri Yolu, Sariyer, 34450, Istanbul, Türkiye
[c] Koç University Surface Science and Technology Center (KUYTAM), Koç University, Rumelifeneri Yolu, Sariyer, 34450, Istanbul, Türkiye

ARTICLE INFO

Keywords:
Mixed matrix membrane (MMM)
Metal-organic framework (MOF)
Acetylene separation
C_2H_2/C_2H_4 separation

ABSTRACT

Separation of acetylene from ethylene is challenging due to the similar physicochemical properties of these two gases. In this regard, the potential of mixed matrix membranes (MMMs) has remained mostly unexplored. Herein, we synthesized MOF/polymer MMMs by incorporating an iron-based metal-organic framework (MOF), MIL-100(Fe), into Pebax polymer matrix at different filler loadings of 10, 15, and 17 wt.%. The synthesized MMMs were characterized in detail and tested for C_2H_2/C_2H_4 separation. Gas permeation measurements showed that the neat Pebax membrane has C_2H_2 and C_2H_4 permeabilities of 434.8 ± 19.0 and 29.6 ± 0.5 Barrer, respectively, at 1 bar and 35 °C, along with the corresponding C_2H_2/C_2H_4 selectivity of 14.7 ± 1. Incorporation of MIL-100(Fe) into the Pebax led to a significant improvement in C_2H_2 permeability and C_2H_2/C_2H_4 selectivity: The MMMs having 15 and 17 wt.% MIL-100(Fe) exhibited C_2H_2 permeabilities of 624.1 ± 5.4 and 509.3 ± 7.3 Barrer, respectively, corresponding to C_2H_2/C_2H_4 selectivities of 23.4 ± 2.3 and 35.6 ± 1.0. Long-term stability tests indicated that the MMMs maintained their separation performance under continuous operation for at least three days, underscoring their robustness and industrial application potential. These results set a benchmark for effectively separating C_2H_2 from C_2H_4 using the synthesized MMMs, offering valuable insights for future acetylene separation applications.

1. Introduction

Acetylene is a critical feedstock in the chemical industry, widely used for the synthesis of high-value chemicals such as vinyl chloride, acrylonitrile, and various polymers [1]. However, the presence of ethylene in acetylene streams can lead to unwanted side reactions and reduce the yield of desired products. Therefore, ensuring the purity of acetylene is essential for maintaining product quality and optimizing the process. The separation of C_2H_2 from C_2H_4 is particularly challenging due to their similar molecular sizes and physicochemical properties [2]. Furthermore, due to its high reactivity, C_2H_2 poses significant safety risks, including the potential for explosive mixtures [3]. As a result, efficient separation technologies are crucial for isolating C_2H_2 from C_2H_4, ensuring the safe handling of these gases while enhancing the production efficiency and purity of the final products.

Cryogenic distillation and catalytic hydrogenation are conventional methods used for C_2H_2/C_2H_4 separation in the industry [4]; however, they require intensive energy and have high operational costs. Membrane-based gas separation technology is more advantageous thanks to its energy-saving characteristics, superior separation properties, and small carbon footprint [5–7]. As in the case of most of the traditional membranes, polymeric membranes are subjected to an inherent trade-off between gas selectivity and permeability, which limits their performance. Mixed matrix membranes (MMMs) combine the easy processability of polymeric membranes with crystalline materials such as zeolites, metal-organic frameworks (MOFs), and covalent-organic frameworks (COFs), generally offering higher selectivity compared to polymer membranes [8,9]. This is owing to their well-defined, uniform pore structures and the presence of functional sites, such as open metal centers in MOFs, which enhance specific interactions with target gases, leading to improved selectivity. These crystalline fillers contribute to improved separation efficiency owing to their high surface area, well-defined pore structures, and tunable chemical properties, which enable selective adsorption and diffusion of target gases. Moreover, the

* Corresponding author. Department of Chemical and Biological Engineering, Koç University, Rumelifeneri Yolu, Sariyer, 34450, Istanbul, Türkiye.
** Corresponding author. Department of Chemical and Biological Engineering, Koç University, Rumelifeneri Yolu, Sariyer, 34450, Istanbul, Türkiye.
E-mail addresses: skeskin@ku.edu.tr (S. Keskin), auzun@ku.edu.tr (A. Uzun).

https://doi.org/10.1016/j.memsci.2025.123782
Received 8 November 2024; Received in revised form 14 January 2025; Accepted 24 January 2025
Available online 26 January 2025
0376-7388/© 2025 The Authors. Published by Elsevier B.V. This is an open access article under the CC BY-NC license (http://creativecommons.org/licenses/by-nc/4.0/).

compatibility between the filler and polymer matrix plays a critical role in maintaining membrane integrity and stability under operational conditions, thereby optimizing both selectivity and permeability [10–12].

Crystalline materials are explored for their potential in C_2H_2/C_2H_4 separation. While pristine MOFs and COFs have been extensively studied for this application [13], their utilization as fillers, particularly in the development of MMMs, is gaining attention. Despite this progress, the membrane separation process of light hydrocarbons is still underdeveloped, and only a few MMMs have been studied to remove acetylene from ethylene [14–16]. For instance, Xu et al. [14] incorporated three different MOFs (MOF-87, -88, and -89) into 6FDA-ODA, a polyimide-based polymer. Among the synthesized MMMs, MOF-89/6FDA-ODA with a filler loading of 15 wt.% exhibited the best performance, achieving the permeabilities of 36.2 Barrer for C_2H_2 and 6.4 Barrer for C_2H_4, corresponding to a C_2H_2/C_2H_4 selectivity of 5.6. These values were superior to the neat membrane having C_2H_2 and C_2H_4 permeabilities of 8 and 3.4 Barrer, respectively, corresponding to C_2H_2/C_2H_4 selectivity of 2.4. Zhang et al. [15] functionalized a COF with an OH anion, followed by MMM synthesis, employing the same polymer (6FDA-ODA) and tested them for C_2H_2/C_2H_4 separation. The C_2H_2 and C_2H_4 permeability of the MMM having 15 wt.% filler loading was increased to 55.6 and 4.6 Barrer, respectively, and the corresponding C_2H_2/C_2H_4 selectivity improved to 12.1. Similarly, the COF nanosheet was incorporated into 6FDA-ODA, and the resulting MMM with 15 wt.% loading showed improved C_2H_2 permeability (10 Barrer) and C_2H_2/C_2H_4 selectivity (6.7) but reduced C_2H_4 permeability (1.5 Barrer) compared to the neat membrane [16]. Therefore, the utilization of MMMs for C_2H_2/C_2H_4 separation offers great potential, though this area still requires extensive investigation.

Pebax, as a polymer matrix, offers high potential thanks to its unique copolymer structure, comprising polyether (PE) and polyamide (PA) segments, which provide the ability to differentiate between gases based on their polarizability and size [17]. C_2H_2 and C_2H_4 gases present distinct challenges in separation due to their close molecular sizes [18]. The soft PE segments provide high flexibility and allow for enhanced diffusivity of smaller, linear molecules like C_2H_2 [19] and offer higher adsorption affinity compared to C_2H_4 thanks to the presence of C≡C bond. Moreover, the rigid PA segments contribute to selective gas separation owing to their tight molecular packing and high density [17]. This structural composition enables Pebax to exploit the size and shape differences between C_2H_2 and C_2H_4, facilitating higher permeability for C_2H_2 and effective separation from C_2H_4 [20]. Furthermore, the PA segments provide thermal and structural stability, essential for maintaining membrane integrity under operational conditions. Pebax's flexibility and resistance to plasticization are particularly advantageous in preventing performance degradation due to high-pressure environments and exposure to reactive gases like C_2H_2, a limitation often observed in more rigid materials such as polyimides [21]. By leveraging these properties, Pebax can achieve effective C_2H_2/C_2H_4 separation, demonstrating its versatility beyond traditional gas pairs. Additionally, Pebax's compatibility with various fillers, such as zeolites and MOFs, offers opportunities to further enhance membrane performance, optimizing selectivity and permeability for this specific application. Based on these, we selected Pebax as the polymer matrix in our study, considering (i) the characteristics of the two gases we aim to separate, (ii) compatibility of Pebax with a wide variety of fillers for the synthesis of MMMs, (iii) its structural and thermal stability, and (iv) our previous experience in manufacturing and characterizating MMMs having Pebax as a polymer matrix [22–24].

As a filler, MIL-100(Fe) (iron (III) trimester) was chosen for its exceptional selective adsorption of C_2H_2, attributed to the strong interactions between acetylene and the framework's unsaturated Fe^{3+} sites and surface hydroxyl groups [25]. These interactions, including π-complexation with the triple bond of C_2H_2, significantly enhance its binding affinity, enabling precise separation. Its high surface area, hierarchical pore structure, and commercial availability further support its practicality for gas separation applications. Besides, the large pores in MIL-100(Fe) provide significant flexibility for post-synthesis modifications, which can be leveraged to further enhance the membrane's performance in subsequent studies.

Based on these reasonings, we incorporated MIL-100(Fe) into the Pebax to synthesize the corresponding MOF/polymer MMMs. The combination of crystalline and amorphous structures in Pebax has the potential to offer high gas permeability, mechanical stability, and the robustness needed for effective gas separation, making it a promising polymer for the MMM application [26]. Our results demonstrated improved separation performance of the resulting MMMs, showcasing significant advancements in membrane-based C_2H_2/C_2H_4 separation. This study provides valuable insights and sets a new benchmark for future research in this challenging field.

2. Materials and methods

2.1. Materials

Pebax 1657 polymer comprised of 60 wt.% polyether oxide (PEO) and 40 wt.% polyamide (PA) was kindly supplied by Arkema. MIL-100 (Fe) was kindly provided by Framergy. Ethanol was purchased from Sigma-Aldrich, and the gases utilized in experiments, including C_2H_2 (99.999 vol%) and C_2H_4 (99.9 vol%), were purchased from Air Liquide.

2.2. Fabrication of MMMs

The MMMs were fabricated by following the procedure reported elsewhere [27]. Prior to the synthesis, the polymer and the MOF were dried in an oven for 12 h to remove any moisture content present. Neat Pebax membrane was synthesized by mixing 4 wt.% of the polymer in an ethanol/water mixture (70/30 wt.%). The mixture was stirred for 4 h at 80 °C until it became homogenous. The membrane was then cast on Teflon substrate and dried in the oven.

For the synthesis of Pebax/MIL-100(Fe) MMMs, a certain amount of MIL-100(Fe) was added to the ethanol/water mixture and stirred for 4 h. Afterwards, MOF suspension was mixed with the polymer-solvent mixture and sonicated for 30 min. The resulting mixture was stirred for 12 h; and then, it was cast and dried in the oven at 35 °C. The temperature was then increased gradually at a rate of 10 °C per hour. Subsequently, the MMMs synthesized were dried at 100 °C in an oven for 12 h and stored in the desiccator. Three different MIL-100(Fe) loadings were considered: 10, 15, and 17 wt.% for the MMMs. When attempting to increase the filler loading to 20 wt.%, the membrane ruptured due to the excessive crystallinity. Therefore, 17 wt.% MIL-100(Fe) loading was set as the highest feasible filler loading for the MMMs synthesized. These membranes were cast into flat sheets with a smooth and uniform surface. The thicknesses were measured using a digital micrometer and found to be 90–110 μm. The typical sizes of the prepared membrane were approximately 9–9.5 cm, consistent across the samples. Their images are included in Fig. S1 of Supplementary Material (SM).

2.3. Characterization

The morphology of the MIL-100(Fe) powder and the cross-sectional morphology of the MMMs were examined by scanning electron microscopy (SEM) analysis. Images were acquired using a Zeiss Evo LS 15 electron microscope with an accelerating voltage of 3 kV. The MMM samples were prepared by freeze-cutting in liquid nitrogen and subsequently coated with a gold layer before analysis.

The mechanical strengths of the neat Pebax and the Pebax/MIL-100 (Fe) MMMs were evaluated using an Instron Electropuls E3000 equipped with pneumatic grips. Tensile strength tests were conducted at a strain rate of 5 mm/min.

X-ray diffraction (XRD) measurements were carried out using a

Rigaku MiniFlex 600 X-ray diffractometer with Kα radiation (λ = 1.5418 Å). The patterns were recorded over a 2θ range of 5–50° with a scanning speed of 1° min^{-1}. Fourier Transform Infrared (FTIR) spectroscopy was conducted using a Bruker Vertex 80v FTIR spectrometer, spanning range of 400–4000 cm^{-1} with a spectral resolution of 2 cm^{-1}. A total of 128 scans were taken for both the background and the sample, respectively. The IR bands were deconvoluted using Fityk software, using the Voigt function [28]. Brunauer-Emmett-Teller (BET) surface area and pore volume measurements of pristine MIL-100(Fe) were performed using a Micromeritics ASAP 2020 adsorption analyzer. The sample was degassed at 200 °C for 12 h before the analysis. N_2 adsorption isotherms were recorded at 78 K over a pressure range from 10^{-6} to 1 bar. The surface area was calculated using the BET equation, and the pore volume was determined using the *t*-plot method.

Thermogravimetric analysis (TGA) was conducted using a TA Instruments Q500 thermogravimetric analyzer equipped with a platinum pan. Nitrogen was used as both the balance and the purge gas, at the corresponding flow rates of 10 mL/min and 90 mL/min, respectively. For the pristine MOF sample, the temperature was initially increased to 120 °C at a rate of 5 °C/min and then held isothermally for 8 h. Subsequently, the temperature was further increased to 700 °C at a ramp rate of 2 °C/min. For the MMM samples, the temperature was raised from room temperature to 700 °C at a heating rate of 5 °C/min. The onset temperature (T_{onset}) and the derivative onset temperature (T'_{onset}) were determined from the thermogravimetric (TG) and derivative thermogravimetric (DTG) curves, respectively. The T_{onset} typically overestimates the actual decomposition temperature, so T'_{onset} was considered as the temperature at which the thermal decomposition starts [29].

2.4. Gas adsorption measurements

Adsorption isotherms of C_2H_2 and C_2H_4 were measured on the MOF, MIL-100(Fe), using a Quantachrome iSorb HP2 volumetric gas adsorption analyzer. Approximately 0.4 g of MIL-100(Fe) was degassed at 200 °C for 12 h under a vacuum of 10^{-6} bar. The isotherms were recorded over a pressure range of 0.1–1 bar, with samples being regenerated at 200 °C for 3 h between measurements. The data were fitted using the Dual-Site Langmuir (DSL) model by employing Ideal Adsorbed Solution Theory (IAST++) software [30], the corresponding fitting parameters are listed in Table S1 of the SM. The adsorption selectivity was calculated by using the following equation,

$$S_{adsorption} = q_i \Big/ q_j \quad (1)$$

where q_i and q_j represent the uptakes of the materials for any gas *i* and *j* at the same pressure and temperature.

2.5. Gas permeation experiments

The gas permeabilities of MMMs were assessed across a pressure difference (ΔP) of 1 bar (upstream pressure at 2 bar and the downstream pressure at 1 bar) at 35 °C using a custom-built experimental setup, as shown in Fig. S2. The flux of the sweeping gas was maintained at 80–100 sccm throughout the experiment to ensure stable operation. For each membrane, measurements were conducted three-times, and the results were reported as the average value with the associated error to ensure accuracy. Performance data were further validated by conducting measurements on multiple batches of the same membrane, with data collected from different batches consistent within less than ±10 %. For long-term stability test, the standard deviation (SD) is also provided. The MMMs were securely sealed in a stainless-steel module with an area of 7 cm^2 using rubber O-rings. The flow rates were controlled using mass flow controllers (MFCs), while a back pressure regulator maintained the upstream pressure at 2 bar and the downstream pressure at 1 bar, ensuring that the measurement was conducted at a ΔP of 1 bar. The downstream pressure was kept at atmospheric pressure. Helium was used to purge residual gases from the system after each test to ensure accurate measurements and continuously flowed as the sweep gas during the experiments. A Hiden Analytical mass spectrometer (QGA gas analyzer) was employed to analyze the composition of the permeate gas. This device was connected to a heated sampling capillary and equipped with a quadrupole mass filter to accurately detect and quantify the gas components. The flux of the permeated gases was calculated based on the data obtained from the mass spectrometric analysis and the sweep gas flow rate.

Gas permeability (Barrer) was calculated using Equation (2), where P_i is the permeability of gas *i*, and J_i the flux (cm^3 (STP)/($s \cdot cm^2$)). Flux is the flow rate of gas, Q_i (cm^3 (STP)/s), divided by the membrane area, A (cm^2). The calculation also incorporates the pressure difference across the membrane, Δ*P* (cm Hg), and membrane thickness, *l* (cm)

$$P_i = (J_i / \Delta P) \times l \quad (2)$$

The membrane selectivity ($S_{i/j}$) was calculated by using equation (3):

$$S_{i/j} = P_i / P_j \quad (3)$$

3. Results and discussion

3.1. Characterization of the materials

The surface area and pore volume of MIL-100(Fe) were determined by measuring N_2 adsorption isotherms presented in Fig. S3 in the SM. The BET surface area and pore volume were calculated as 1258 cm^2/g and 0.67 cm^3/g, respectively, which are comparable to the literature values [31–33]. The SEM images of the pristine MIL-100(Fe) are presented in Fig. 1(a) and (b) at magnifications of 2 k× and 6.9 k×, respectively. The pristine MIL-100(Fe) demonstrated some degree of agglomeration, with the crystals lacking perfect geometric uniformity. This agglomeration resulted in an average MIL-100(Fe) aggregate size of around 21 μm ((see Fig. S4(a)), calculated from the SEM images provided in Fig. 1(a). The lack of uniformity in crystal geometry, as reported in the literature [34], was also noted.Fig. S4(a). However, the synthesis procedure involving 4 h of constant stirring followed by 30 min of sonication effectively disperses these aggregates, yielding MIL-100(Fe) particles (Fig. 1(c), presenting a representative SEM image of the filler after the sonication step) with an average particle size of 1.2–1.3 μm, as illustrated in Fig. S4(b). Despite the presence of irregular shapes and sizes, which deviate from the ideal octahedral structure typically associated with MIL-100(Fe), the crystals still exhibit distinct characteristics of the MOF.

Similarly, the cross-sectional morphology of synthesized MIL-100 (Fe)/Pebax MMMs having 10, 15, and 17 wt.% filler loading was also analyzed. The corresponding SEM images collected at different positions are presented in Fig. 2(a), (b), and (c) (at a magnification of 10 k ×) and in Fig. 2(d), (e), and (f) (at a magnification of 20 k×). It was observed that at all filler loadings, MIL-100(Fe) particles are uniformly distributed within the polymer matrix with no evidence of phase separation or dual-layer formation. Similarly, the EDS mapping provided in Fig. S5 confirms that the Fe distribution, corresponding to MIL-100(Fe), is homogeneous across the MMM surfaces for all filler loadings (10, 15, and 17 wt.%), indicating the effective dispersion of the MIL-100(Fe) particles within the Pebax matrix. Additionally, the Fe signal intensity increases proportionally with higher filler loadings, as expected, reflecting the increased concentration of MIL-100(Fe) in the MMMs. Such consistent and uniform distribution, even at high filler loadings, demonstrates the successful integration of the filler into the membrane without signs of aggregation. The SEM analysis further revealed that at a filler loading of 17 wt.% (as shown in Fig. 2(c) and (f)), the MMM exhibits a slight roughness associated with the relatively high concentration of MIL-100 (Fe) particles. Moreover, detailed surface characterization of the 17 wt. % MIL-100(Fe)/Pebax MMM at various magnifications demonstrated

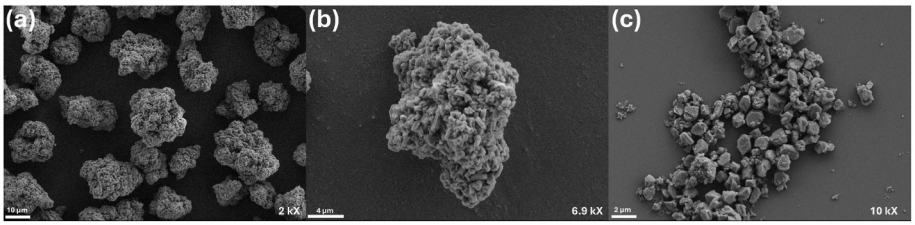


Fig. 1. SEM images of MIL-100(Fe): (a) Pristine MIL-100(Fe) at 2 k× magnification, (b) Pristine MIL-100(Fe) at 6.9 k× magnification, and (c) Sonicated MIL-100(Fe) at 10 k× magnification. A comparison of the corresponding particle size distributions is presented in Fig. S4.

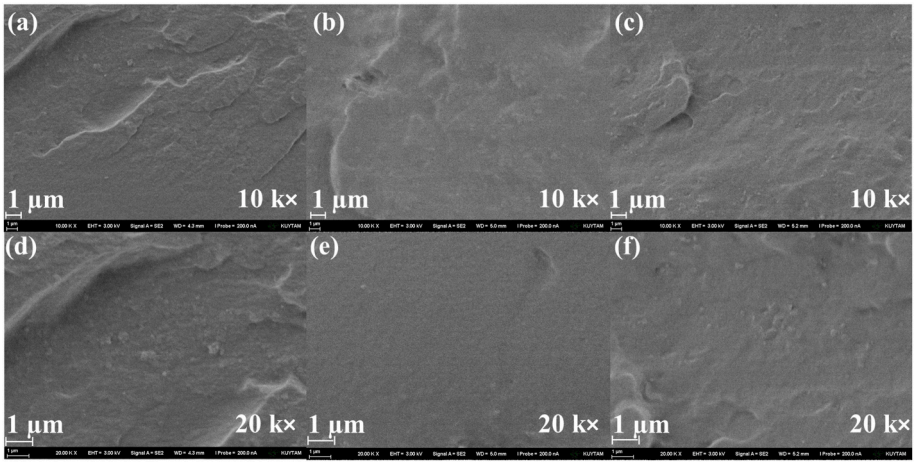


Fig. 2. SEM images of MIL-100(Fe)/Pebax MMMs having a MIL-100(Fe) loading of (a) 10 wt.%, (b) 15 wt.%, (c) 17 wt.% at a magnification of 10 k× and (d) 10 wt. %, (e) 15 wt.%, and (f) 17 wt.% at a magnification of 20 k× .

the homogeneous distribution of MIL-100(Fe) particles without any agglomeration after casting (see Fig. S6(a)), preserving their reduced particle size achieved through stirring and sonication, as observed in Fig. 1(c). Similarly, investigation of the filler-polymer matrix interface at 50 k× , 100 k× , and 200 k× magnifications in Figs. S6(b–d) illustrated the defect-free structure of the 17 wt.% MIL-100(Fe)/Pebax MMM, with no evidence of cracks or interfacial pore formation. However, as the filler loading was increased to 20 wt.%, the membrane exhibited significant cracking, likely due to the excessive crystallinity and the challenges of uniform dispersion of filler particles at such a high filler concentration [35,36]. Therefore, in this study, 17 wt.% loading was selected as the highest filler loading to achieve a defect-free MMM along with the improved separation performance.

The stress-strain characteristics of neat Pebax and MIL-100(Fe)/Pebax MMMs are investigated in Fig. S7. Data show that addition of MIL-100(Fe) as a filler significantly enhances the mechanical properties of the Pebax membrane. Accordingly, the Young's modulus increases from 49.8 MPa for neat Pebax to 74.7 MPa for a filler loading of 10 wt.% (Table S2). We speculate that this increase is associated with the efficient stress transfer between the polymer matrix and the well-dispersed filler, which also improves tensile strength and durability under high-pressure conditions. However, at higher filler loadings of 15 and 17 wt.%, the Young's modulus decreases to 64.6 and 59.2 MPa, respectively, likely because of a possible filler agglomeration, which reduces homogeneity, flexibility, and tensile strength.

The XRD diffractograms of pristine MIL-100(Fe), neat Pebax, and MOF-100(Fe)/Pebax MMMs are shown in Fig. 3(a). The characteristic XRD peaks of pristine MIL100(Fe) located at $2\theta = 5.8$, 6.2, 6.7, 10.1, 10.9, and 20° are well-matched with the reported literature [37,38], confirming the structural integrity of the MOF. In the XRD patterns of membranes, the neat Pebax showed a broad peak around $2\theta = 12$–24°, which can be ascribed to the polyamide (PA) group present in the polymer [23,39]. The characteristic peak associated with the PA group was also observed in all the MMMs. In the case of MOF-100(Fe)/Pebax MMMs, new peaks were observed at $2\theta = 10.1$, 10.9, and 20°, which were associated with the pristine MIL-100(Fe), with no apparent shifts in their peak positions. Additionally, as the MOF loading was increased from 10 to 17 wt.%, the intensities of the peaks associated with MIL-100 (Fe) were observed to increase, corresponding to an increase in the crystallinity of the resulting MMMs, as expected.

TGA analyses were conducted on MIL-100(Fe), neat Pebax, and the synthesized MOF/polymer MMMs as shown in Fig. 3(b), to determine their thermal stability limits. The TGA profile of pristine MIL-100(Fe) showed a three-step decomposition profile matching well with the literature [40,41]. First weight loss up to T'_{onset} of 395 °C corresponds to the removal of water molecules that are coordinated with the MIL-100 (Fe) structure. The second weight loss occurs at a T'_{onset} of approximately 440 °C, which was attributed to the decomposition of the organic ligand. Finally, the third and final stage, with a T'_{onset} between 515 and 600 °C, is ascribed to the complete collapse of the MIL-100(Fe) framework [32,42]. In contrast, the neat Pebax membrane and the MMMs presented in Fig. 3(b) exhibited a single-step decomposition mechanism, with initial degradation starting at T'_{onset} temperature of 350 °C, and the complete collapse of polymer backbone at T'_{onset} of 420 °C. All MMMs displayed a similar decomposition pattern, and thermal stability up to 350 °C, demonstrating high thermal resilience. Moreover, with the addition of MIL-100(Fe) in Pebax, a slight change was observed in the DTG curves, possibly indicating some interactions between the MOF and the polymer.

To gain insights into these interactions, an analysis based on IR spectroscopy was conducted. The IR spectra of the pristine MIL-100(Fe), the neat Pebax, and the synthesized MMMs were analyzed to investigate the interactions between the MOF and the polymer, as shown in Fig. 3 (c). In the IR spectra of MIL-100(Fe), the peaks located at 710 and 760 cm^{-1} were ascribed to ν[C–H] stretching vibration of the benzene ring [32]. Moreover, the characteristic peaks present at 1380, 1450, and

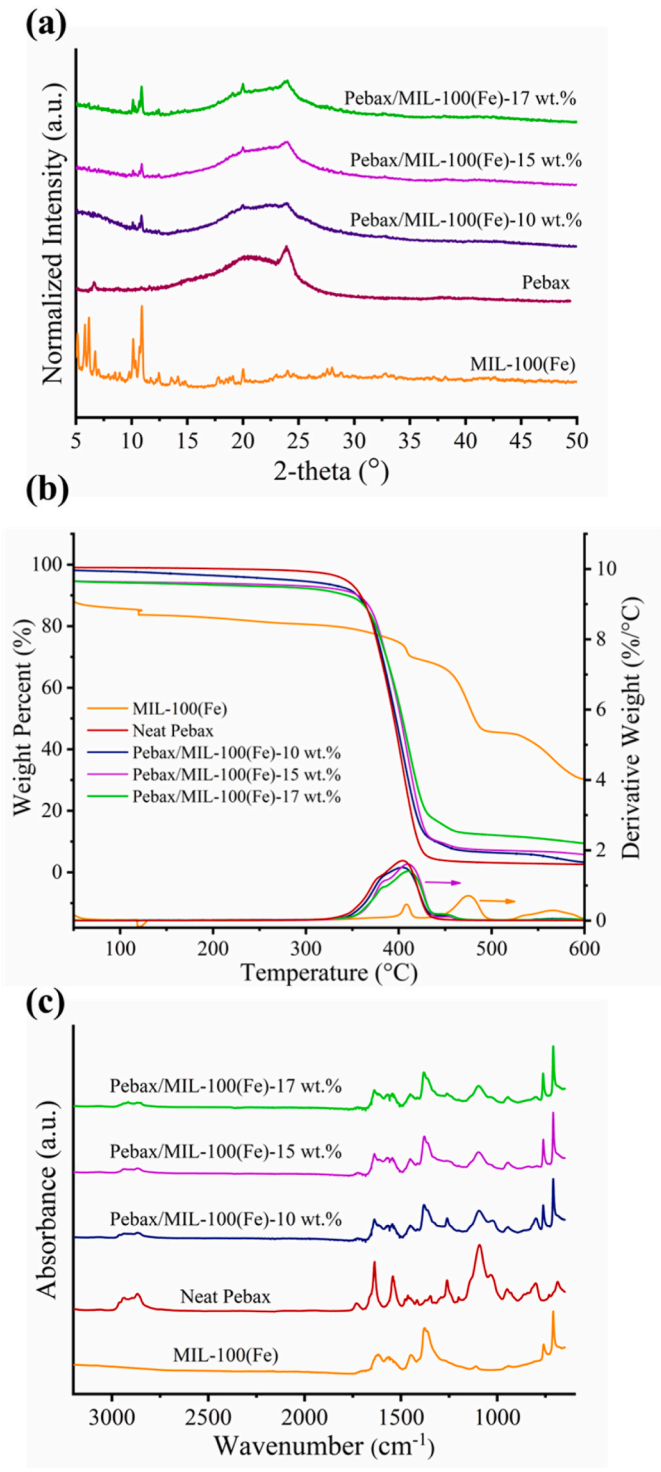


Fig. 3. (a) XRD diffractogram, (b) TGA and DTG curves, and (c) IR spectra of MIL-100(Fe), neat Pebax, and MIL-100(Fe)/Pebax MMMs at 10, 15, and 17 wt. % loadings.

1560 cm^{-1} were associated with the ν[C–O] stretching vibrations. The band located at 1630 cm^{-1} was ascribed to the C═O of the benzene-1,3, 5-tricarboxylate (BTC) linker present in the MIL-100(Fe). The broad peak located around 2900 to 3600 cm^{-1} representing ν[O–H] stretching vibrations was ascribed to the coordination of water molecules with open metal sites of MIL-100(Fe) [43].

In the IR spectra of neat Pebax membrane presented in Fig. 3(c), the characteristic peaks located at 1097, 1636, and 1731 cm^{-1} corresponded to ν(C–O–C) vibrations, ν(O–C–O), and ν(H–N–C═O) vibrations, of PEO segment, respectively. The peaks located at 1541 and 2948 cm^{-1} were ascribed to the ν(N–H) vibrations of the PA groups within the polymer structure [22]. All the characteristic peaks of Pebax polymer were present in the MMMs; however, a change in the intensity of the peaks was observed, which can be ascribed to the interaction between the polymer and the MOF particles, affecting the overall polymer membrane structure. Besides, new peaks were observed at wavenumbers of 710, 762, 1381, and 1573 cm^{-1} in the IR spectra of the MMMs, compared to the spectrum of the neat Pebax. These new bands were associated with the characteristic IR peaks of the pristine MIL-100 (Fe) as described above. A slight blue shift of 2 cm^{-1} was observed in the position of the ν(C–H) compared to its corresponding position in the pristine MIL-100(Fe) spectrum. Moreover, the peak at 1573 cm^{-1} associated with ν(C–O) stretching vibrations in the MIL-100(Fe) structure presented a blue shift of 13 cm^{-1} compared to its position in the IR spectrum of the pure MOF. This shift indicates that the ligand present in the MOF structure is interacting with the polymer. Moreover, the peak corresponded to the PEO group of the polymer present at 1639 cm^{-1} also showed a blue shift of 3 cm^{-1} (slightly higher than the spectral resolution) in the MMMs. These shifts in the position of the IR features associated with the polymer functional groups and the linker of the MOF likely indicate the presence of weak van der Waals interactions between the MOF and polymer within the membrane structure.

3.2. Gas separation performances of the materials

3.2.1. Adsorption-based gas separation

Volumetric gas adsorption isotherms for single-component C_2H_2 and C_2H_4 for MIL-100(Fe) and neat Pebax membrane were measured at pressures ranging from 0.01 to 1 and 0.01–0.5 bar, respectively, at 25 °C, as illustrated in Fig. 4(a) and Fig. S8. The C_2H_2 and C_2H_4 isotherms were fitted using the Dual-Site Langmuir (DSL) employing the IAST++ software, the corresponding fitting parameters are given in Table S1. The C_2H_2 and C_2H_4 uptakes of MIL-100(Fe) were measured as 1.7 and 0.8 cm^3/g, respectively, at 0.01 bar. As the pressure was increased to 1 bar, gas uptakes were increased to 36 and 30 cm^3/g for C_2H_2 and C_2H_4, respectively, which are consistent with values reported in the literature [44]. The gas uptake behavior of the neat Pebax membrane with a thickness of 0.09 mm presented in Fig. S8(a) reveals a strong affinity for C_2H_2 over C_2H_4, as evident from the higher C_2H_2 adsorption capacity (3.5 cc STP/g at 0.5 bar) compared to C_2H_4 (approximately 0.5 cc STP/g). This trend highlights the material's preferential interaction with acetylene.

The corresponding C_2H_2/C_2H_4 adsorption selectivities at different pressures were computed for MIL-100(Fe) and neat Pebax membrane based on the fitting parameters, as shown in Fig. 4(b) and Fig. S8(b). MIL-100(Fe) demonstrated the C_2H_2/C_2H_4 selectivity of 2.2 at 0.01 bar. However, as the pressure was increased to 1 bar, the selectivities decreased to 1.2. The reduction in selectivity can be attributed to the transition in the gas adsorption mechanism. At low pressures, adsorption is predominantly influenced by specific interactions between the gas molecules and the active sites on the surface of MIL-100(Fe), which enhance the selectivity. In contrast, at higher pressures, the adsorption mechanism shifts, and the process is primarily governed by the availability of pore volume rather than specific interactions [45,46], resulting in a decrease in selectivity. Comparative analysis indicates that the C_2H_2 uptake and C_2H_2/C_2H_4 selectivity values for MIL-100(Fe) align well with those reported for other C_2H_2 selective MOFs in the literature, as detailed in Table S3. Moreover, the ideal C_2H_2/C_2H_4 selectivity of the Pebax membrane decreases with increasing pressure, starting from 14 at low pressures and stabilizing near 8 at 0.5 bar, confirming the neat Pebax membrane's potential for C_2H_2/C_2H_4 separation.

3.2.2. Membrane-based gas separation

Pure gas permeability measurements for C_2H_2 and C_2H_4 were

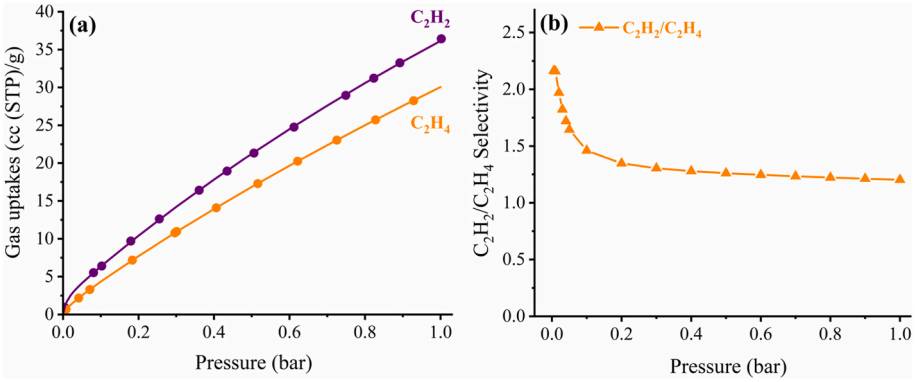


Fig. 4. (a) Volumetric C_2H_2 and C_2H_4 uptakes measured at 25 °C and up to 1 bar. (b) C_2H_2/C_2H_4 adsorption selectivity of MIL-100(Fe). In (a), circles indicate the experimental data, while the lines represent the fitted isotherms.

conducted for neat Pebax and the MIL-100(Fe)/Pebax MMMs at 1 bar and 35 °C, as depicted in Fig. 5(a). Based on permeability data, the corresponding C_2H_2/C_2H_4 selectivities of membranes were calculated as presented in Fig. 5(b). The data are also provided in tabular form in Table S4 in the SM. For the neat Pebax membrane, C_2H_2 and C_2H_4 permeabilities were measured as 434.8 ± 19.0 and 29.6 ± 0.5 Barrer, respectively, with the corresponding C_2H_2/C_2H_4 selectivities of 14.7 ± 1.0.

In the case of MIL-100(Fe)/Pebax MMMs, it was observed that the addition of MIL-100(Fe) improved the C_2H_2 permeabilities along with the C_2H_2/C_2H_4 selectivities, as shown in Fig. 5. For instance, the MMM having 10 wt.% MIL-100(Fe) loading exhibited C_2H_2 and C_2H_4 permeabilities of 528.0 ± 26 and 30.5 ± 4.5 Barrer, respectively, along with the corresponding C_2H_2/C_2H_4 selectivity of 17.3 ± 1.7. As the MIL-100 (Fe) loading was increased to 15 wt.%, C_2H_2 permeability was further increased to 624.1 ± 5.4 Barrer, along with the C_2H_4 permeability of 26.7 ± 3.0 Barrer, corresponding to a C_2H_2/C_2H_4 selectivity of 23.4 ± 2.3. Thus, the MMM having 15 wt.% filler loading demonstrated a 1.4-times improvement in C_2H_2 permeability and 1.6-times higher C_2H_2/C_2H_4 selectivity, compared to the neat Pebax membrane.

The C_2H_2/C_2H_4 selectivity of the MMM was further improved to 35.6 ± 1 with an increase in filler loading to 17 wt.%. This selectivity corresponds to a 2.4-times improvement compared to that of the neat Pebax. This improvement can be attributed to several factors, primarily associated with the differences in the interaction strengths of the two gases with the MIL-100(Fe) structure. C_2H_2 molecules exhibit stronger van der Waals and Lewis acid-base interactions with the unsaturated Fe^{3+} centers and surface hydroxyl (OH) groups present in MIL-100(Fe) compared to C_2H_4 molecules. This difference facilitates the enhanced adsorption of C_2H_2, which is crucial for improving the membrane's C_2H_2 selectivity over C_2H_4 [25]. However, the improvement in selectivity at high filler loading occurs at the expense of reduction in permeabilities (to 509.3 ± 7.3 and 14.3 ± 1.2 Barrer for C_2H_2 and C_2H_4, respectively). This behavior is attributed to the agglomeration of MOF particles or interfacial defects within the membrane matrix, which may obstruct gas transport pathways [35]. Therefore, we posit that the optimal balance of filler loading is crucial to maximize the performance of the MMM in gas separation applications.

Well-established gas separation mechanisms for MMMs are extensively discussed in the literature. Researchers, including Xu et al. [14] and Yin et al. [47], suggest that polymer membranes and MMMs separate gases primarily through the solution-diffusion mechanism. In MMMs, gas molecules undergo additional adsorption and diffusion through the filler materials, enhancing separation. In contrast, neat polymer membranes rely solely on solution and diffusion through the matrix. The separation of C_2H_2 and C_2H_4 by Pebax and MIL-100 (Fe)/Pebax MMMs follows the same model. For the neat Pebax membrane, separation occurs via solution-diffusion, driven by the differential solubility and diffusivity of the gases. Upon incorporating MIL-100(Fe), the separation mechanism becomes more complex. The MOF filler introduces gas-surface interactions and a molecular sieving effect. Gas molecules adsorb onto the MOF and diffuse through its pores, enhancing separation by selectively filtering C_2H_2 and C_2H_4 based on size and adsorption affinity. As the filler loading increases from 10 to 17 wt.%, the MOF's contribution grows, shifting from the polymer's solution-diffusion mechanism to a hybrid mechanism that combines polymer and MOF effects. This transition significantly boosts separation performance, highlighting the potential of MIL-100(Fe) filler in enhancing gas separation [14].

The interaction of C_2H_2 with Pebax/MIL-100(Fe) MMMs were further investigated by IR spectroscopy. Fresh membranes were compared with C_2H_2-saturated membranes to elucidate the interaction

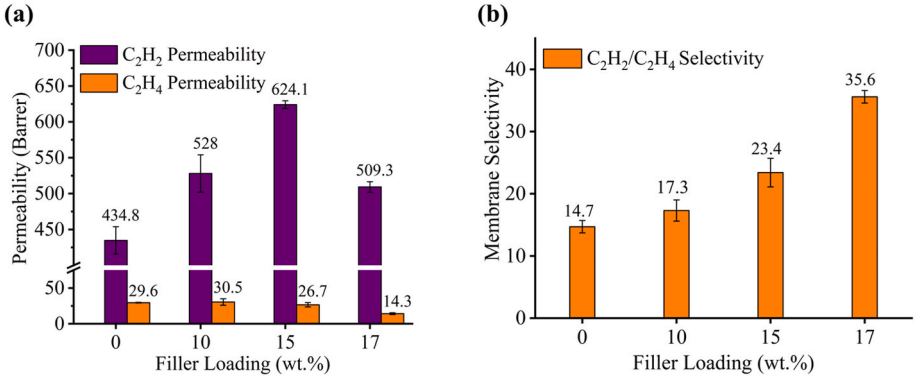


Fig. 5. (a) C_2H_2 and C_2H_4 permeabilities, (b) C_2H_2/C_2H_4 selectivities of MIL-100(Fe)/Pebax MMMs compared to neat Pebax, measured at 35 °C and a feed pressure of 1 bar.

mechanism. The peaks at 710 and 760 cm^{-1}, corresponding to the ν(C–H) stretching vibrations of the benzene rings in the BTC linker [32], exhibit a decrease in intensity when the MMMs are saturated with C_2H_2 as shown in Fig. S9. Based on this observation, we speculate that the benzene rings in the BTC linker have interactions with C_2H_2, potentially through π-π interactions. It is possible that the electron-rich triple bond of acetylene interacts with the delocalized π-electrons of the benzene rings and slightly alters the strengths of C–H and C–C bonds. Additionally, appearance of new peaks at lower wavenumbers could indicate a deconvolution of the IR features, potentially arising from modified vibrational modes of the aromatic system introduced by the saturation of acetylene.

Next, we compared our data with the existing literature to evaluate the performance of our MMMs with the previously reported relevant membranes for C_2H_2 and C_2H_4 separation in Table S5. For instance, a MOF-89/6FDA-ODA MMM having a filler loading of 15.2 wt.% exhibited a C_2H_2 permeability of 36.2 Barrer [14]. In another study, a COF nanosheets/6FDA-ODA MMM showed a C_2H_2 permeability of 10 Barrer [16]. The C_2H_2 permeability of our 15 wt.% MIL-100(Fe)/Pebax MMM (624.1 ± 5.4 Barrer) was measured as approximately 17-times higher than that of MOF-89/6FDA-ODA MMM, and about 62-times higher than the COF nanosheets/6FDA-ODA MMM. Similarly, it is over 11-times higher compared to that of a COF iPAF-1-OH/6FDA-ODA MMM having a filler loading of 15 wt.% (55.6 Barrer) [15]. Additionally, the C_2H_2/C_2H_4 selectivity of the MIL-100(Fe)/Pebax MMM having a filler loading of 17 wt.% (35.6 ± 1.0) is also significantly higher than those of MOF-89/6FDA-ODA MMM (5.6) [14], COF iPAF-1-OH/6FDA-ODA (12.1) [15], and COF nanosheet/6FDA-ODA MMM (6.7) [16]. Another study investigated the performance of the NaA–NaX zeolite membrane. The synthesized NaA–NaX membrane shows significantly enhanced performance for C_2H_2/C_2H_4 separation, with a C_2H_2 permeance of 24.9 Barrer and a C_2H_2/C_2H_4 selectivity of 3.2 [48]. These comparisons illustrate the exceptional performance of MIL-100(Fe)/Pebax MMMs synthesized in this work for acetylene separation.

To check the reproducibility and the long-term stability of the MMMs, we prepared another batch of the MMM with 17 wt.% MIL-100 (Fe) loading and tested its separation performance. The comparison of the acetylene separation performance of this new batch with the first one confirmed the perfect reproducibility of the MMM. Subsequently, the long-term stability was assessed over a time-on-stream of 75 h under identical operating conditions. Data provided in Fig. S10 demonstrated that the MMM exhibited stable C_2H_2 and C_2H_4 permeabilities within an error range of less than ±8%, the corresponding average values were determined as 565.8 ± 45 with a standard deviation of 28.7 and 14.2 ± 2 with a standard deviation of 0.9 Barrer, respectively. Similarly, as Fig. 6 shows, the C_2H_2/C_2H_4 selectivity remained constant at 39.8 ± 3 (with a standard deviation of 1.9). Moreover, to assess the integrity of the MMM before and after this long-term measurement, XRD analysis was conducted on the used MMM. The results presented in Fig. S11 showed the lack of any significant changes in the peak positions of the MIL-100(Fe)/Pebax MMM, confirming that the membrane maintained its structural integrity throughout the test, further supporting its robust performance for C_2H_2/C_2H_4 separation. This stability is particularly notable given the challenging nature of the separation of the gas pair.

4. Conclusion

In this study, Pebax/MIL-100(Fe) MMMs with various filler loadings were synthesized and tested for selective separation of C_2H_2 from C_2H_4. The MIL-100(Fe) exhibited an exceptional affinity for acetylene, driven by the strong interactions with the Fe^{3+} and surface OH sites, leading to favorable separation of C_2H_2 over C_2H_4. The gas permeation experiments conducted at 1 bar and 35 °C showed that the neat Pebax has permeabilities of 434.8 ± 19.0 and 29.6 ± 0.5 Barrer for C_2H_2 and C_2H_4, respectively, along with a C_2H_2/C_2H_2 selectivity of 14.7 ± 1.0. Incorporating MIL-100(Fe) into the Pebax membrane enhanced its C_2H_2 permeability and C_2H_2/C_2H_4 selectivity. The MMMs containing 15 and 17 wt.% MIL-100(Fe) demonstrated C_2H_2 permeabilities of 624.1 ± 5.4, and 509.3 ± 7.3 Barrer, respectively, with corresponding C_2H_2/C_2H_4 selectivities of 23.4 ± 2.3 and 35.6 ± 1.0, respectively. The best performance was achieved with 17 wt.% MIL-100(Fe) loading, setting a new benchmark for C_2H_2/C_2H_4 separation. With only a handful of previous studies in the literature focusing on this separation using MMMs, our work establishes a new standard in the field by leveraging the unique properties of MIL-100(Fe) within a new polymer matrix, addressing the challenging task of C_2H_2/C_2H_4 separation.

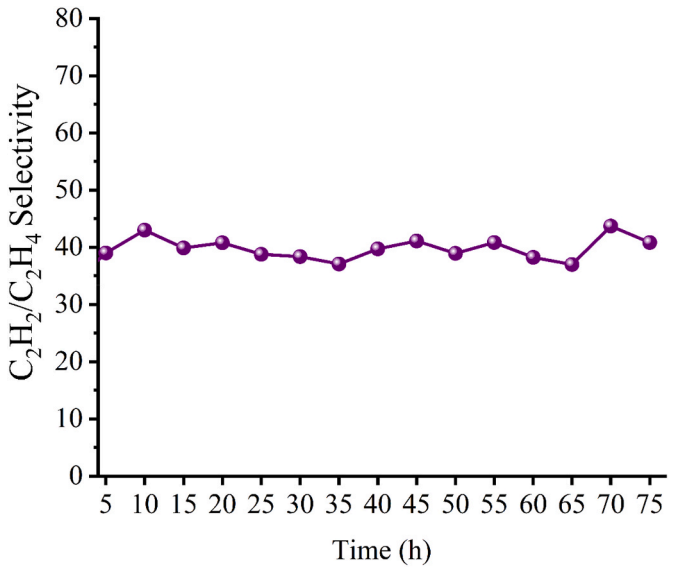


Fig. 6. Variation of C_2H_2/C_2H_4 selectivity of MIL-100(Fe)/Pebax MMM having a filler loading of 17 wt.% over a time-on-stream of 75 h at 35 °C and 1 bar.

CRediT authorship contribution statement

Nitasha Habib: Writing – review & editing, Writing – original draft, Visualization, Validation, Methodology, Investigation, Formal analysis, Data curation, Conceptualization. **Ahmet Safa Aydogdu:** Writing – review & editing, Visualization, Validation, Methodology, Investigation, Formal analysis, Data curation. **Seda Keskin:** Writing – review & editing, Writing – original draft, Supervision, Resources, Methodology, Investigation, Funding acquisition, Formal analysis, Conceptualization. **Alper Uzun:** Writing – review & editing, Writing – original draft, Supervision, Resources, Methodology, Investigation, Funding acquisition, Formal analysis, Conceptualization.

Declaration of competing interest

The authors declare that they have no known competing financial interests or personal relationships that could have appeared to influence the work reported in this paper.

Acknowledgements

The authors acknowledge the support of Koç University TÜPRAŞ Energy Center (KUTEM), Koç University Surface Science and Technology Center (KUYTAM). A.U. acknowledges the Fulbright Türkiye's Visiting Scholar Program and the Scientific and Technological Research Council of Türkiye (TUBITAK) 2219 Program. The authors thank Tuğser Yılmaz and Asst. Prof. Umut Aydemir of the Koç University Boron and Advanced Materials Application and Research Center (KUBAM) for their help in XRD measurements.

Appendix A. Supplementary data

Supplementary data to this article can be found online at https://doi.org/10.1016/j.memsci.2025.123782.

Data availability

Data will be made available on request.

References

[1] H. Steiner, Introduction to Petroleum Chemicals: Based on Lectures Given at the Manchester College of Science and Technology, Elsevier, 2015.
[2] H. Molero, B. Bartlett, W. Tysoe, The hydrogenation of acetylene catalyzed by palladium: hydrogen pressure dependence, J. Catal. 181 (1) (1999) 49–56.
[3] Y. Ji, L. Ding, Y. Cheng, H. Zhou, S. Yang, F. Li, Y. Li, Understanding the effect of ligands on C_2H_2 storage and C_2H_2/CH_4, C_2H_2/CO_2 separation in metal–organic frameworks with open Cu (II) sites, J. Phys. Chem. C 121 (43) (2017) 24104–24113.
[4] F.G. Kerry, Industrial Gas Handbook: Gas Separation and Purification, CRC press, 2007.
[5] Q. Qian, P.A. Asinger, M.J. Lee, G. Han, K. Mizrahi Rodriguez, S. Lin, F. M. Benedetti, A.X. Wu, W.S. Chi, Z.P. Smith, MOF-based membranes for gas separations, Chem. Rev. 120 (16) (2020) 8161–8266.
[6] C.-H. Kang, Y.-F. Lin, Y.-S. Huang, K.-L. Tung, K.-S. Chang, J.-T. Chen, W.-S. Hung, K.-R. Lee, J.-Y. Lai, Synthesis of ZIF-7/chitosan mixed-matrix membranes with improved separation performance of water/ethanol mixtures, J. Membr. Sci. 438 (2013) 105–111.
[7] G. Dong, H. Li, V. Chen, Challenges and opportunities for mixed-matrix membranes for gas separation, J. Mater. Chem. A 1 (15) (2013) 4610–4630.
[8] S. Miri, M. Omidkhah, A.E. Amooghin, T. Matsuura, Membrane-based gas separation accelerated by quaternary mixed matrix membranes, J. Nat. Gas Sci. Eng. 84 (2020) 103655.
[9] M. Aroon, A. Ismail, T. Matsuura, M. Montazer-Rahmati, Performance studies of mixed matrix membranes for gas separation: a review, Separ. Purif. Technol. 75 (3) (2010) 229–242.
[10] N. Habib, Z. Shamair, N. Tara, A.-S. Nizami, F.H. Akhtar, N.M. Ahmad, M.A. Gilani, M.R. Bilad, A.L. Khan, Development of highly permeable and selective mixed matrix membranes based on Pebax® 1657 and NOTT-300 for CO_2 capture, Separation and Purification Technology 234 (2020) 116101.
[11] N. Tara, Z. Shamair, N. Habib, M. Craven, M.R. Bilad, M. Usman, X. Tu, A.L. Khan, Simultaneous increase in CO_2 permeability and selectivity by BIT-72 and modified BIT-72 based mixed matrix membranes, Chem. Eng. Res. Des. (2021).
[12] M.S. Buddin, A. Ahmad, A review on metal-organic frameworks as filler in mixed matrix membrane: recent strategies to surpass upper bound for CO_2 separation, J. CO2 Util. 51 (2021) 101616.
[13] S. Qian, L. Xia, L. Yang, X. Wang, X. Suo, X. Cui, H. Xing, Defect-free mixed-matrix membranes consisting of anion-pillared metal-organic frameworks and poly (ionic liquid) s for separation of acetylene from ethylene, J. Membr. Sci. 611 (2020) 118329.
[14] T. Xu, P. Zhang, F. Cui, J. Li, L. Kan, B. Tang, X. Zou, Y. Liu, G. Zhu, Fine-tuned ultra-microporous metal–organic framework in mixed-matrix membrane: pore-tailoring optimization for C_2H_2/C_2H_4 separation, Adv. Mater. 35 (13) (2023) 2204553.
[15] P. Zhang, X. Zou, J. Song, Y. Tian, Y. Zhu, G. Yu, Y. Yuan, G. Zhu, Anion substitution in porous aromatic frameworks: boosting molecular permeability and selectivity for membrane acetylene separation, Adv. Mater. 32 (30) (2020) 1907449.
[16] J. Li, Z. Cheng, Z. Wang, J. Dong, H. Jiang, W. Wang, X. Zou, G. Zhu, Ultramicroporous covalent organic framework nanosheets with functionality pair for membrane C_2H_2/C_2H_4 separation, Angew. Chem. 135 (10) (2023) e202216675.
[17] J.H. Kim, S.Y. Ha, Y.M. Lee, Gas permeation of poly (amide-6-b-ethylene oxide) copolymer, J. Membr. Sci. 190 (2) (2001) 179–193.
[18] W. He, X.-B. Mu, J. Lei, W. Yuan, P. Zhang, Q.-G. Zhai, Novel pillared-layer-like metal–organic frameworks with quadrilateral channels for efficient separation of C_2H_2 from C_2H_2/CO_2 and C_2H_2/C_2H_4 mixtures, Cryst. Growth Des. 23 (6) (2023) 4346–4356.
[19] C. Staudt-Bickel, W.J. Koros, Olefin/paraffin gas separations with 6FDA-based polyimide membranes, J. Membr. Sci. 170 (2) (2000) 205–214.
[20] J. Hou, P. Liu, M. Jiang, L. Yu, L. Li, Z. Tang, Olefin/paraffin separation through membranes: from mechanisms to critical materials, J. Mater. Chem. A 7 (41) (2019) 23489–23511.
[21] J. Krol, M. Boerrigter, G. Koops, Polyimide hollow fiber gas separation membranes: preparation and the suppression of plasticization in propane/propylene environments, J. Membr. Sci. 184 (2) (2001) 275–286.
[22] N. Habib, O. Durak, M. Zeeshan, A. Uzun, S. Keskin, A novel IL/MOF/polymer mixed matrix membrane having superior CO_2/N_2 selectivity, J. Membr. Sci. 658 (2022) 120712.
[23] N. Habib, Ö. Durak, A. Uzun, S. Keskin, Incorporation of a pyrrolidinium-based ionic liquid/MIL-101 (Cr) composite into Pebax sets a new benchmark for CO_2/N_2 selectivity, Separation and Purification Technology 312 (2023) 123346.
[24] N. Habib, I. Tarhanlı, E. Senses, S. Keskin, A. Uzun, IL-modified MOF-177 filler boosts the CO_2/N_2 selectivity of Pebax membrane, J. Membr. Sci. 710 (2024) 123143.
[25] J.W. Yoon, J.S. Lee, S. Lee, K.H. Cho, Y.K. Hwang, M. Daturi, C.H. Jun, R. Krishna, J.S. Chang, Adsorptive separation of acetylene from light hydrocarbons by mesoporous iron trimesate MIL-100 (Fe), Chem.–Eur. J. 21 (50) (2015) 18431–18438.
[26] M.A. Wahab, A. Sunarti, Development of PEBAX based membrane for gas separation: a, Int. J. 2 (2) (2015) 79.
[27] N. Habib, I. Tarhanlı, E. Senses, S. Keskin, A. Uzun, IL-modified MOF-177 filler boosts the CO_2/N_2 selectivity of Pebax membrane, J. Membr. Sci. (2024) 123143.
[28] M. Wojdyr, Fityk: a general-purpose peak fitting Program, J. Appl. Crystallogr. 43 (5-1) (2010) 1126–1128.
[29] A. Akçay, V. Balci, A. Uzun, Structural factors controlling thermal stability of imidazolium ionic liquids with 1-n-butyl-3-methylimidazolium cation on γ-Al_2O_3, Thermochim. Acta 589 (2014) 131–136.
[30] S. Lee, J.H. Lee, J. Kim, User-friendly graphical user interface software for ideal adsorbed solution theory calculations, Kor. J. Chem. Eng. 35 (1) (2018) 214–221.
[31] J. Liao, D. Wang, A. Liu, Y. Hu, G. Li, Controlled stepwise-synthesis of core–shell Au@ MIL-100 (Fe) nanoparticles for sensitive surface-enhanced Raman scattering detection, Analyst 140 (24) (2015) 8165–8171.
[32] M. Nehra, N. Dilbaghi, N.K. Singhal, A.A. Hassan, K.-H. Kim, S. Kumar, Metal organic frameworks MIL-100 (Fe) as an efficient adsorptive material for phosphate management, Environ. Res. 169 (2019) 229–236.
[33] J. Panda, S.N. Sahu, R. Pati, P.K. Panda, B.C. Tripathy, S.K. Pattanayak, R. Sahu, Role of pore volume and surface area of Cu-BTC and MIL-100 (Fe) metal-organic frameworks on the loading of rifampicin: collective experimental and docking study, ChemistrySelect 5 (40) (2020) 12398–12406.
[34] N.E. Elharony, I.E.T. El Sayed, A.G. Al-Sehemi, A.A. Al-Ghamdi, A.S. Abou-Elyazed, Facile synthesis of iron-based MOFs MIL-100 (Fe) as heterogeneous catalyst in kabachnick reaction, Catalysts 11 (12) (2021) 1451.
[35] W. Chen, Z. Zhang, C. Yang, J. Liu, H. Shen, K. Yang, Z. Wang, PIM-based mixed-matrix membranes containing MOF-801/ionic liquid nanocomposites for enhanced CO_2 separation performance, J. Membr. Sci. 636 (2021) 119581.
[36] M.J.C. Ordonez, K.J. Balkus Jr., J.P. Ferraris, I.H. Musselman, Molecular sieving realized with ZIF-8/Matrimid® mixed-matrix membranes, J. Membr. Sci. 361 (1–2) (2010) 28–37.
[37] V.C. Nguyen, H.T. Nguyen, H.D. Tran, T.N. Tu, W.-S. Kim, J. Kim, Facile synthesis of bimetallic MIL-100 (Fe, Al) for enhancing CO_2 Adsorption performance, Microporous Mesoporous Mater. 360 (2023) 112716.
[38] B. Yuan, X. Wang, X. Zhou, J. Xiao, Z. Li, Novel room-temperature synthesis of MIL-100 (Fe) and its excellent adsorption performances for separation of light hydrocarbons, Chem. Eng. J. 355 (2019) 679–686.
[39] L. Xiang, Y. Pan, G. Zeng, J. Jiang, J. Chen, C. Wang, Preparation of poly (ether-block-amide)/attapulgite mixed matrix membranes for CO_2/N_2 separation, J. Membr. Sci. 500 (2016) 66–75.
[40] D. Ozer, O. Icten, N. Altuntas-Oztas, B. Zumreoglu-Karan, MIL-100 (Fe) metal–organic framework catalyzed oxidation of phenol revisited: dark-Fenton activity of the catalyst, Res. Chem. Intermed. 46 (2020) 909–922.
[41] A. Bhattacharjee, M.K. Purkait, S. Gumma, Doxorubicin loading capacity of MIL-100 (Fe): effect of synthesis conditions, J. Inorg. Organomet. Polym. Mater. 30 (2020) 2366–2375.
[42] M.A. Simon, E. Anggraeni, F.E. Soetaredjo, S.P. Santoso, W. Irawaty, T.C. Thanh, S. B. Hartono, M. Yuliana, S. Ismadji, Hydrothermal synthesize of HF-free MIL-100 (Fe) for isoniazid-drug delivery, Sci. Rep. 9 (1) (2019) 16907.
[43] S. Rostamnia, H. Alamgholiloo, Synthesis and catalytic application of mixed valence iron (Fe II/Fe III)-based OMS-MIL-100 (Fe) as an efficient green catalyst for the aza-Michael reaction, Catal. Lett. 148 (2018) 2918–2928.
[44] H.S. Scott, M. Shivanna, A. Bajpai, D.G. Madden, K.-J. Chen, T. Pham, K.A. Forrest, A. Hogan, B. Space, J.J. Perry IV, Highly selective separation of C_2H_2 from CO_2 by a new dichromate-based hybrid ultramicroporous material, ACS Appl. Mater. Interfaces 9 (39) (2017) 33395–33400.
[45] B. Koyuturk, C. Altintas, F.P. Kinik, S. Keskin, A. Uzun, Improving gas separation performance of ZIF-8 by [BMIM][BF_4] incorporation: interactions and their consequences on performance, J. Phys. Chem. C 121 (19) (2017) 10370–10381.
[46] F.P. Kinik, C. Altintas, V. Balci, B. Koyuturk, A. Uzun, S. Keskin, [BMIM][PF_6] incorporation doubles CO_2 selectivity of ZIF-8: elucidation of interactions and their consequences on performance, ACS Appl. Mater. Interfaces 8 (45) (2016) 30992–31005.
[47] H. Yin, A. Alkaş, Y. Zhang, Y. Zhang, S.G. Telfer, Mixed matrix membranes (MMMs) using an emerging metal-organic framework (MUF-15) for CO_2 separation, J. Membr. Sci. 609 (2020) 118245.
[48] H. Rong, J. Zhang, Y. Guan, D. Gai, X. Zou, Interzeolite conversion-synthesized sub-1 μm NaA zeolite membrane for C_2H_2/C_2H_4 selective separation, ACS Appl. Mater. Interfaces 14 (22) (2022) 26171–26179.